

Article

Surface Modification of Pure Mg for Enhanced Biocompatibility and Controlled Biodegradation: A Study on Graphene Oxide (GO)/Strontium Apatite (SrAp) Biocomposite Coatings

Oktay Yigit ¹, Turan Gurgenc ², Burak Dikici ^{3,*}, Mosab Kaseem ⁴, Carl Boehlert ⁵ and Ersin Arslan ⁶

¹ Department of Metallurgical and Materials Engineering, Firat University, Elazig 23119, Turkey; oyigit@firat.edu.tr

² Department of Automotive Engineering, Firat University, Elazig 23119, Turkey; tgurgenc@firat.edu.tr

³ Department of Metallurgical and Materials Engineering, Ataturk University, Erzurum 25240, Turkey

⁴ Department of Nanotechnology and Advanced Materials Engineering, Sejong University, Seoul 05006, Republic of Korea; mosabkaseem@sejong.ac.kr

⁵ Department of Chemical Engineering and Materials Science, Michigan State University, East Lansing, MI 48824, USA; boehlert@egr.msu.edu

⁶ Department of Mechanical Engineering, Istanbul Aydin University, Istanbul 34295, Turkey; ersinarslan@aydin.edu.tr

* Correspondence: burakdikici@atauni.edu.tr; Tel.: +90-442-231-6030

Abstract: Magnesium alloys have excellent biodegradability but suffer from high corrosion rates and unfavorable biological responses. Thus, a surface modification strategy to regulate the corrosion rate and enhance biocompatibility is required. In this study, pure Mg substrate surfaces were coated with strontium apatite (SrAp) and graphene oxide (GO) biocomposite structures using the hydrothermal method to increase the biocompatibility of the surface of the Mg and obtain a moderate biodegradation rate. The effect of the GO concentration (0, 2, 4, and 6 wt.%) on the surface microstructure and its corrosion behavior were systematically studied. The corrosion behavior of the coatings was characterized in-vitro using the electrochemical polarization method in Hank's solution. An EDS-connected SEM was used to examine the coatings' surface properties. The functional groups of the coatings were identified using ATR-IR spectroscopy. To determine the degree of crystallization and examine the elemental distribution of the coatings, an XRD was used with a grazing incidence attachment. The XRD and SEM-EDS results showed that increasing the GO ratio in the SrAp-based coatings significantly enhanced the homogeneity and crystallinity, and the ATR-IR spectroscopy revealed that the SrAp/GO coatings were rich in functional groups, including hydroxyl, phosphate, and carbonate groups, that are known to promote bone formation and regeneration. The results of the electrochemical polarization tests demonstrated a considerable decrease in the corrosion rates for the samples with SrAp matrix and GO coatings. Additionally, the coatings containing GO exhibited higher polarization resistance (R_p) values, indicating their potential as a promising surface modification technique for biodegradable implants. These findings suggest that incorporating GO into the SrAp coatings could enhance their biocompatibility and provide a moderate biodegradation rate, which is desirable for biomedical applications.

Keywords: pure Mg; surface modification; hydrothermal; graphene oxide (GO); strontium apatite (SrAp); in-vitro corrosion



Citation: Yigit, O.; Gurgenc, T.; Dikici, B.; Kaseem, M.; Boehlert, C.; Arslan, E. Surface Modification of Pure Mg for Enhanced Biocompatibility and Controlled Biodegradation: A Study on Graphene Oxide (GO)/Strontium Apatite (SrAp) Biocomposite Coatings. *Coatings* **2023**, *13*, 890. <https://doi.org/10.3390/coatings13050890>

Academic Editors: Liqiang Wang and James Kit-Hon Tsoi

Received: 6 April 2023

Revised: 5 May 2023

Accepted: 6 May 2023

Published: 9 May 2023



Copyright: © 2023 by the authors. Licensee MDPI, Basel, Switzerland. This article is an open access article distributed under the terms and conditions of the Creative Commons Attribution (CC BY) license (<https://creativecommons.org/licenses/by/4.0/>).

1. Introduction

Biodegradable metallic implant materials are a relatively new area of research and development in biomedical engineering. These materials are designed to be absorbed by the human body over time, eliminating the need for a second surgical operation to remove the implant. The main advantage of these materials is that they reduce the risk of implant-related complications and provide a more natural healing process [1].

Recent studies showed that the most popular biodegradable materials are iron (Fe), magnesium (Mg), and zinc (Zn) metals and their alloys [1]. In addition, several clinical studies have evaluated the performance of biodegradable (or bioresorbable) metallic implants, and the results have been encouraging [1–3].

Mg alloys have various advantages compared to other biodegradable alloys such as Fe and Zn. Firstly, magnesium has high biocompatibility and no toxic effects on the body. Additionally, magnesium alloys have a low density, making them lightweight, and they have excellent mechanical properties [4]. Therefore, they are very promising for use in implants and other orthopedic applications. Mg alloys have the potential to be used in orthopedic, cardiovascular, and dental implants, among other applications. However, due to the high rate of corrosion and rapid dissolution of Mg alloys, they may not be suitable for long-term use. Thus, further research is needed to optimize their properties and degradation rates for specific biomedical applications. Alternatively, surface modification techniques have been developed to improve biocompatibility and control the biodegradation rate of Mg-based implants [5]. Several studies have investigated the surface modification of Mg-based implants with different materials, including calcium phosphate (CaP), hydroxyapatite (HA), and biodegradable polymers [6–9]. Graphene oxide (GO) and strontium apatite (SrAp) have recently received significant attention for their potential biomedical applications. GO is a two-dimensional carbon material with a high surface area, excellent mechanical properties, and biocompatibility [10]. SrAp, a bioactive ceramic material, has been shown to enhance bone formation and promote osteogenesis [11].

There are several coating techniques used for coating biodegradable Mg alloys to increase bioactivity, including electrodeposition [12], sol-gel [13], plasma spraying [14], physical vapor deposition (PVD) [15], chemical vapor deposition (CVD) [16], plasma electrolytic oxidation (PEO) [17], or hydrothermal treatment [8]. The specific technique used depends on the desired properties of the coating and the intended application.

Among these methods, hydrothermal treatment is a surface modification technique that has gained attention in recent years for coating biodegradable Mg alloys. One of the major advantages of hydrothermal treatment is that it allows for the formation of a uniform and compact coating with good adhesion to the substrate [18]. Additionally, hydrothermal treatment helps to prevent damage to the underlying substrate [19]. Coatings synthesized by hydrothermal treatment have been found to enhance the corrosion resistance and biocompatibility of biodegradable Mg alloys [20]. For example, hydrothermal synthesis was used to deposit strontium phosphate (Sr-P) coatings on Mg, and the effect of the treatment temperature on the properties of coatings was investigated by Kavitha et al. [21]. The results showed that an increase in treatment temperature from 80 to 200 °C led to an increase in coating weight, density, and crystallinity, resulting in higher corrosion resistance in the Hank's solution. In another study, Wu et al. [22] investigated the fabrication of reduced-GO (rGO) reinforced apatite composite layers on Mg alloy using the hydrothermal method to improve the bonding strength and corrosion resistance of the apatite layer. The results confirmed the successful incorporation of GO into the layer during the hydrothermal process. The rGO/apatite layer is a feasible method to improve the bonding strength and corrosion resistance of hydrothermal layers, making them more practical for clinical applications.

Protective bioactive strontium-substituted hydroxyapatite (Sr-HA) coatings were synthesized by Yang and Wang [23] using the hydrothermal synthesis technique on the biodegradable AZ91D Mg alloy. The hydrophilicity of the Mg substrate was demonstrated by executing alkaline and hydrothermal treatments, and the hydrothermally produced Sr-HA conversion coating exhibited a surface topography with nanoscale flake-like crystallites. Immersion studies showed that the Sr-HA coating provided the Mg alloy with long-term stability, resulting in a decrease in the concentration of released Mg^{2+} ions in the simulated bodily fluid (SBF), as well as a reduction in the rate of corrosion. Furthermore, polarization tests showed that the nanostructured Sr-HA-coated specimens had superior corrosion resistance compared with specimens that had the HA coating.

To date, the combination of SrAp and GO has not been extensively investigated for Mg-based implants. This study aims to fill this gap in the literature and provide insights into the potential use of SrAp and GO as a biocomposite coating for Mg-based implants.

In this study, we aimed to enhance the biocompatibility and control the biodegradation rate of Mg-based implants by coating the pure Mg substrate surfaces with a biocomposite of SrAp and GO using the hydrothermal method. In addition, the effect of GO concentration on the surface microstructure and the in-vitro corrosion susceptibility of the coatings was systematically investigated.

2. Experimental Procedures

2.1. Materials

Pure Mg (99.99%) substrates were carefully prepared by cutting 5 mm thick samples from 12 mm diameter bar samples by wire-erosion. To remove the natural oxide layer formed on the surface of the pure Mg substrates, a series of SiC sandpapers ranging from 600 to 1200 grit were used for polishing. The polished substrates were then subjected to a 30 min ultrasonic bath in acetone and ethanol, respectively, to eliminate any remaining contaminants. Afterward, the surfaces were thoroughly cleaned with deionized water and dried with hot air for 10 min to ensure that the substrates were free of any residues. To form the SrP/GO composites, the following three different materials were used: strontium nitrate ($\text{Sr}(\text{NO}_3)_2$) (purity 99.995%, Sigma-Aldrich, Darmstadt, Germany), di-ammonium hydrogen phosphate ($\text{H}_9\text{N}_2\text{O}_4\text{P}$) (purity > 99%, Merck, Darmstadt, Germany), and graphene oxide (purity 99.8%, NanoGrafi, Ankara, Turkey) as sources of strontium, phosphate, and graphene, respectively.

2.2. Hydrothermal Synthesis of Biocomposite Coatings

In preparation for coating, the prepared pure Mg samples were fixed vertically in the middle of the Teflon liner inside the hydrothermal reaction vessel. A two-step solution was prepared for the hydrothermal synthesis. The first solution consisted of 0.2 M $\text{Sr}(\text{NO}_3)_2$ in 25 mL of deionized water, while the second solution contained 0.12 M $\text{H}_9\text{N}_2\text{O}_4\text{P}$ in 25 mL of deionized water. Finally, both solutions were mixed using a magnetic stirrer for 30 min at room temperature to ensure homogeneous dissolution. Three GO suspensions were prepared with different ratios of 2, 4, and 6 wt.% in 10 mL of deionized water using an ultrasonic homogenizer (Sonopuls, Bandelin, Berlin, Germany). While stirring, the second solution was then added dropwise to the first solution, and the GO solution was added last. A magnetic stirrer was used to mix the resultant suspension, and an ammonia solution was then added while stirring for 60 min at room temperature to increase the pH level to 11. The 60 mL suspension was stirred for another 30 min before being transferred to a Teflon-coated autoclave for hydrothermal treatment. The hydrothermal reaction was maintained at 180 °C for 4 h in a PID-controlled hydrothermal device (Fytronix FYHT-8000, Elazig, Turkiye). A previous study showed that a 200 °C treatment temperature provided an increase in coating weight, density, and crystallinity [21]. The samples were dried in a vacuum oven at 80 °C and 50 mbar pressure for one hour following the hydrothermal synthesis. Figure 1 offers a schematic illustration of the procedure.

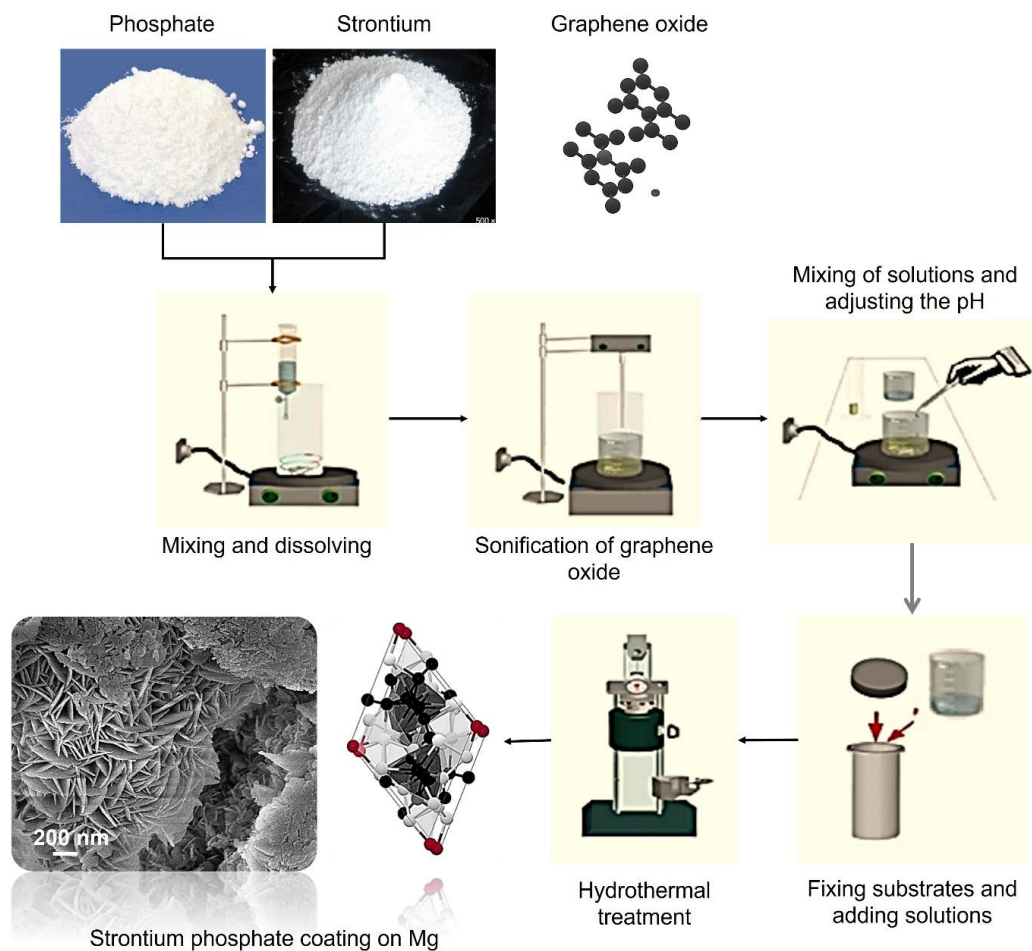


Figure 1. A schematic representation of the hydrothermal synthesis process.

2.3. In-Vitro Corrosion Tests

The in-vitro corrosion responses of the coatings were investigated using a potentiostat/galvanostat (Gamry, PCI14/750, Warminster, PA, USA). The corrosion experiments were performed using the following three standard electrodes: saturated silver/silver chloride (Ag/AgCl) (reference), platinum (Pt) wire (counter), and coated Mg samples (working electrode). A standard potentiodynamic scanning (PDS) procedure [24] was used in the electrochemical studies of the coatings. The corrosion tests were performed with Hank's solution at body temperature (37 ± 0.5 °C) and at a pH of about 7.4. The open circuit potentials (E_{ocp}) of the coated Mg samples were monitored until they attained a steady-state potential. Then, the polarization scan was started with a rate of $1 \text{ mV}\cdot\text{s}^{-1}$ from the cathodic overpotential of 0.3 V vs. E_{ocp} . The scan was stopped when the specimens reached an indicated anodic current density ($10 \text{ mA}\cdot\text{cm}^{-2}$). The covered surface area of the samples was calculated to be approximately 1.13 cm^2 , and all data were normalized with respect to the surface area. Afterward, the samples for which PDS tests were performed were ultrasonically cleaned with ethanol to remove the waste products from the corroded surfaces. Echem Analyst software (v.5.50, ©Gamry Instruments) was used to compare the corrosion rates of the coated samples in accordance with ASTM G102 [25].

2.4. Characterizations

Using a grazing incidence X-ray diffraction (GI-XRD, PANalytical Empyrean, Malvern, UK) apparatus and monochromatic Cu-K α radiation (λ : 0.15406 nm) under the following condition, 40 kV, 40 mA, 0.5° GI angle, and scan rate at $0.02 \text{ deg}\cdot\text{s}^{-1}$ from 10 to 80° , the phase structure of SrP/GO-based composite coatings was examined. The XRD results, peak intervals, and phase structure were defined using X'Pert Highscore plus software (v.2.2b,

PANalytical B.V.). The functional groups of the composite coatings were investigated using attenuated total reflection infrared (ATR-IR) spectroscopy (Thermo Scientific™, Nicolet™ iS™5, Waltham, MA, USA). Scans were completed for each coating in the range of 500–4000 cm^{-1} , with a spectral resolution of 0.5 cm^{-1} . Surface morphologies of the coatings before and after the corrosion tests, elemental analyses of SrAp/GO structures, and the formation of SrAp and GO structures on the surface were obtained using a field emission scanning electron microscope (FE-SEM, Jeol, JSM-7001F, Tokyo, Japan) outfitted with secondary electrons and energy dispersive spectroscopy (EDS, Inca system, Bucks, UK) below 15 kV. The thickness of the coatings was measured using an optical profilometer, and an atomic force microscopy (AFM, Park System 100-E, Tokyo, Japan) analysis was conducted on the coated surfaces to determine their surface roughness.

3. Results and Discussion

The phase compositions of the SrAp-based coatings formed on the pure Mg substrates were analyzed using X-ray diffraction (XRD) as depicted in Figure 2.

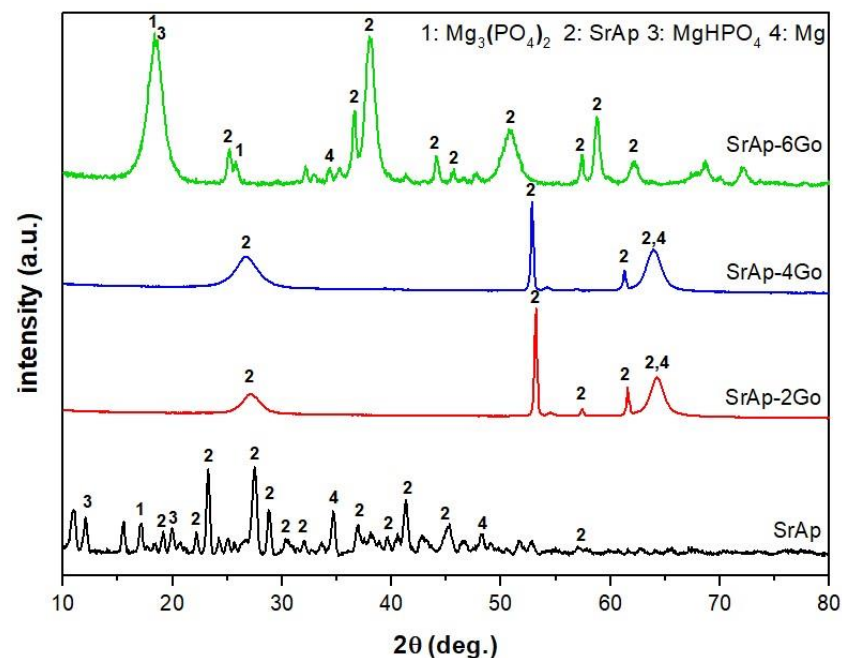


Figure 2. X-ray diffraction (XRD) intensity versus two-theta plot of the SrAp-based coatings synthesized on the pure Mg substrates.

The XRD analysis revealed that the addition of GO to the coatings resulted in the formation of new phases, including $\text{Mg}_3(\text{PO}_4)_2$, MgHPO_4 , SrAp, and Mg, as indicated by the appearance of distinctive peaks in the XRD patterns. Moreover, the crystallinity of these phases increased with the addition of GO, and the intensities of the SrAp and MgHPO_4 phases became more pronounced, indicating a significant enhancement of these phases in the presence of GO. The most notable changes were observed in the coatings with 6 wt.% GO addition. These results are in good agreement with previously reported studies [26–28]. These findings suggest that GO can effectively improve the phase composition and crystallinity of SrAp-based coatings, which could lead to the enhanced mechanical and biological properties.

The FT-IR spectra of SrAp-based and GO-doped biocomposite coatings are provided in Figure 3.

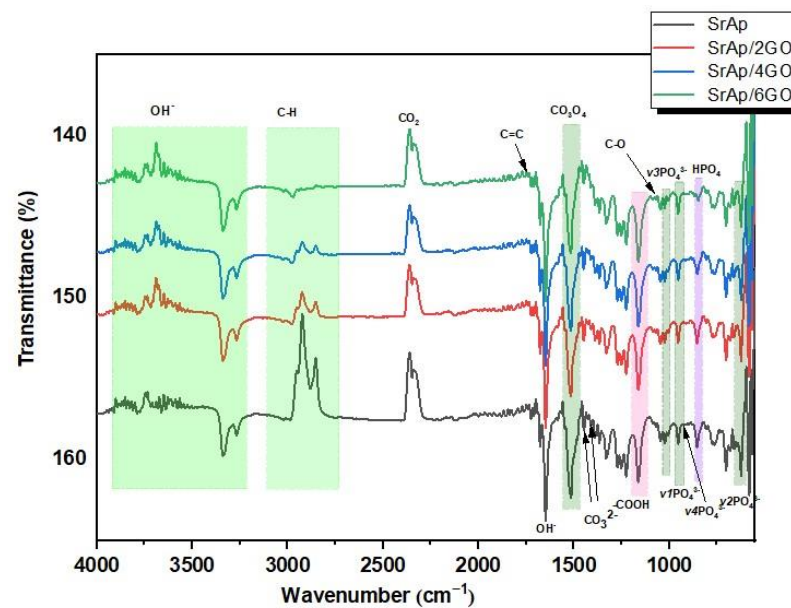


Figure 3. The FT-IR spectra of SrAp-based and GO-doped biocomposite coatings.

GO structures gain chemical functionality as a result of the incorporation of functional oxygen groups into the composite, and they exhibit an sp^3 -hybridized carbon structure (with hydroxyl and ether/epoxy functional groups on both sides of the surfaces) and sp^2 -hybridized carbon structure (carbonyl and carboxyl functional groups on both surfaces and edges) [29]. The bands corresponding to the CO bonds of GO at 1161 cm^{-1} can be seen in Figure 3. The presence of the carboxyl groups seen from the peaks was confirmed by stretching vibrations of the carbonyl group in the range of 1720 to 1740 cm^{-1} . This was also seen with the bending mode of the hydroxyl groups between 1620 and 1640 cm^{-1} . The hydroxyl group was formed due to the antisymmetric and symmetric extensions of the C-H groups with bands between 2740 and 3100 cm^{-1} . A significant decrease in the peaks in this range was observed with the increase in the GO additive. The main reason for this decrease is the increase of C-O functional groups and the formation of more functional groups with the increase of GO [29].

Characteristic absorption bands of phosphate, hydroxyl, and carbonate-based groups can be seen in the SrAp-GO nanocomposite spectra provided in Figure 3. The broadband between 3900 and 3200 cm^{-1} was associated with adsorbed water due to the OH^- groups' intermolecular and intramolecular tension bands. The band at 1650 cm^{-1} was attributed to the vibrational mode of O-H-O bonds. The symmetrical stretching vibration mode in the 3200 – 3900 cm^{-1} confirmed the existence of hydroxyl groups. During hydrothermal synthesis in an aqueous environment, carbonate bands (CO_3^{2-}) can replace anionic sites in the SrAp structure, as observed in bands at 1456 and 1417 cm^{-1} . The band at about 870 cm^{-1} confirmed the HPO_4^{2-} phase [21,30]. Well-defined bands at 1017 , 951 , and 917 cm^{-1} were assigned to the ν_3 stretching vibration, ν_1 asymmetrical stretching vibration, and ν_4 asymmetric bending band of the PO_4^{3-} group, respectively. Furthermore, bands at 623 and 567 cm^{-1} were observed, and these corresponded to the ν_2 asymmetric deformation of the same group [31].

A decrease in peak intensity between 3100 and 2700 cm^{-1} was observed in the adsorbed water band, with the addition of 6 wt.% GO. There was also some decrease in the GO carbonyl group bands. This decrease in peak intensities can be explained by the accumulation and interaction of the SrAp nanostructures between the functionalized surface groups of the GO sheets. In light of these results, the binding of hydroxyl structures to the functional surface groups of GO proves the existence of a strong interaction between the SrAp structures and the GO, in agreement with the SEM analysis described below.

Figures 4 and 5 show FE-SEM images of SrAp/GO composites at low and higher magnifications, respectively.

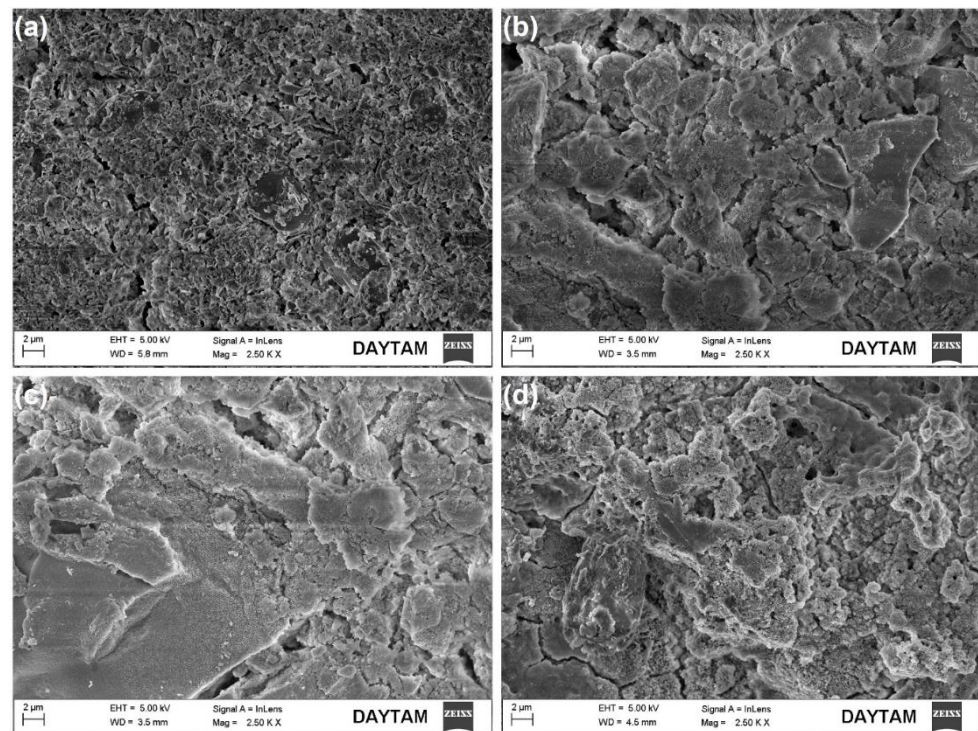


Figure 4. FE-SEM secondary electron surface images of SrAp/GO biocomposite coatings: (a) SrAp, (b) SrAp/2GO, (c) SrAp/4GO, and (d) SrAp/6GO.

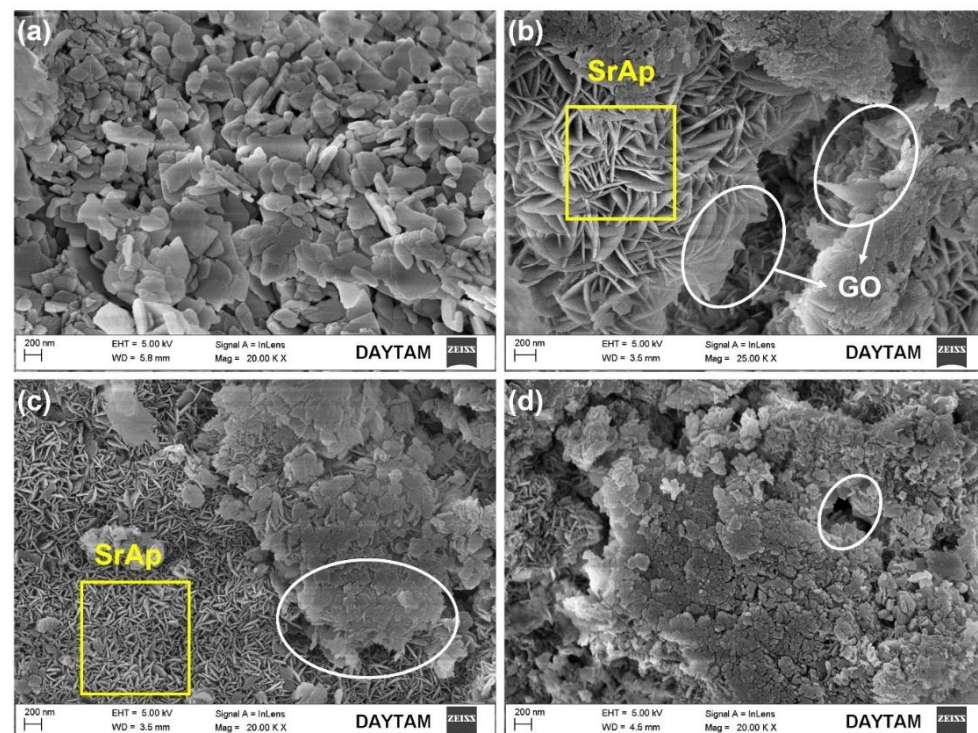


Figure 5. FE-SEM surface images of SrAp/GO biocomposite coatings at higher magnification: (a) SrAp, (b) SrAp/2GO, (c) SrAp/4GO, and (d) SrAp/6GO (the yellow squares indicate regions containing SrAp, while the white ovals indicate regions containing the GO).

SrAp nanoparticles adhered to the GO layers' surface, indicating that there is a strong affinity between SrAp and GO. The amount of SrAp on the GO layer surfaces increased as the functional groups of the GO structure increased. Therefore, the interaction between the SrAp and GO increased. The GO-free SrAp-based coating morphology shows a diffuse and highly porous surface feature on the pure Mg alloy surface (see Figure 4). The SrAp-based coating exhibited a fine-grained structure.

As a result of the addition of GO, a composite coating structure was obtained, and the SrAp structures on the coated surface began to show a more compact and coarser structure. Due to the GO layers being present in the composite, the SrAp structures, which have a relatively large bonding area, exhibited a porous composite form with increased surface roughness. The rougher surfaces obtained in the composite coatings and the presence of the porous morphology were primarily caused by interactions of the nano-sized SrAp structures with the functional groups in the GO layers during the coating stage. Such coatings formed from the hydrothermal process. Two of the most important reasons why the hydrothermal method is preferred in such biological coatings are that the surface properties of the SrAp crystals obtained by this method can be controlled under different conditions, and the SrAp/GO-based coatings can be produced in different morphologies. This coating, with high porosity and rough surfaces, created with SrAp/GO nanoparticles, allows cell structures, such as osteoblasts and fibroblasts, to more easily adhere to the surface. This is preferred for implant applications [32]. A schematic illustration of the potential for utilizing GO/SrAp biocomposite coatings on pure Mg to improve biocompatibility and regulate biodegradation is presented in Figure 6.

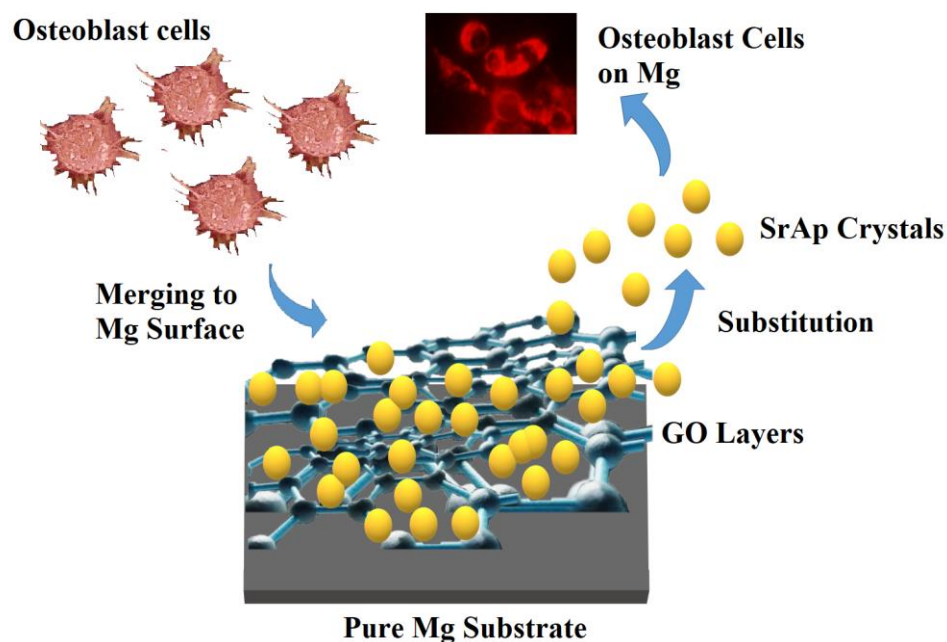


Figure 6. A schematic illustration of the potential for utilizing GO/SrAp biocomposite coatings on pure Mg.

When the amount of GO additive in the coatings increased, nanostructures started to develop and the GO layers on the surfaces could be more clearly observed. The SrAp crystals, seen as thick plates, started to take the form of thin leaves at high (20,000 \times) magnification. With an increasing GO ratio, as seen in Figure 5b–d, the SrAp crystals became prominent. The size of the SrAp structures decreased from the microscale to the nanoscale. The SrAp crystals indicated heterogeneous nucleation spots within the GO layers, which were the fundamental causes of the transition from their microscale to their nanoscale and the shift in crystal morphologies. By adding GO to the composite, the SrAp structure was subsequently produced as nanosheets during the recrystallization, which

occurred during the hydrothermal process. Coatings made with a 2 wt.% GO additive exhibited a coarser and relatively less homogeneous structure than coatings with 4 and 6 wt.% GO additions (see Figure 5b). More graphene oxide layers were produced in the composite structure as the GO content increased, and more functional groups were added to the structure. Therefore, the SrAp crystals were exhibited more nucleation and were smaller in size with an increased GO content. Increased GO additives resulted in the formation of surface structures that were coarser and more permeable. Nevertheless, the coating on the surface became denser. In hydrothermal synthesis studies, it has been reported that nanostructures proliferate between GO layers in composites from which the nanocomposites are produced [33,34].

Nanoscale SrAp needles with a 10–20 nm thickness and a diameter of about 150 nm were visible on the surface; see Figure 5b,c. A more detailed image of the square marked area in Figure 5c is provided in Figure 7.

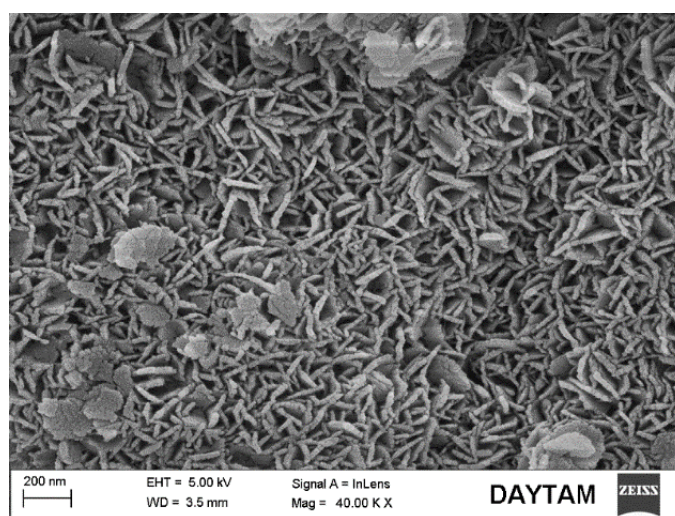


Figure 7. FE-SEM image of the yellow square marked area of SrAp/4GO biocomposite coating in Figure 5c.

The number of SrAp crystals in the coatings increased significantly, and their size decreased when no GO was present. The structures with large clusters were GO layers; see Figure 5c,d. The formation of leaf-shaped SrAp structures on the GO layers was particularly striking. These structures looked like flower petals. The increase in the GO additive caused the increase in the number of SrAp crystals [33,35]. Similar GO layers have been observed in other studies [36]. The structures of the GO-doped SrAp composites were consistent with the XRD and FT-IR analyses. It was noted that even at higher GO concentrations, no agglomeration of the GO sheets was observed.

The elemental composition of pure Mg samples coated with the SrAp/GO composite was determined using an EDS analysis; see Figure 8.

In Figure 8, Sr, P, O, and Mg were seen on the sample surface consistent with the GO-free coating. The content of Sr and P was relatively high, and the signal from Mg was low. The reason for this was the formation of a coarse SrAp structure on the surface and a poor reading of the signals from the substrate. On the other hand, the presence of C, O, Sr, P, and Mg elements in GO-added composites supported the existence of SrAp/GO compounds. Thus, it has been observed that the structures growing in the form of nano leaves/needles can be successfully grown on the GO surfaces and interlayers. In addition, the increase in the carbon with increased GO in the composite structures supports the presence of GO in the composite. Signals from the Mg substrate were increased in these coatings. An increased Mg peak height resulted from the more porous and compact coating. Overall, the EDS results suggest that hydrothermal synthesis, which allows for the control of the chemical ratios, can be a successful method for producing biomedical coatings.

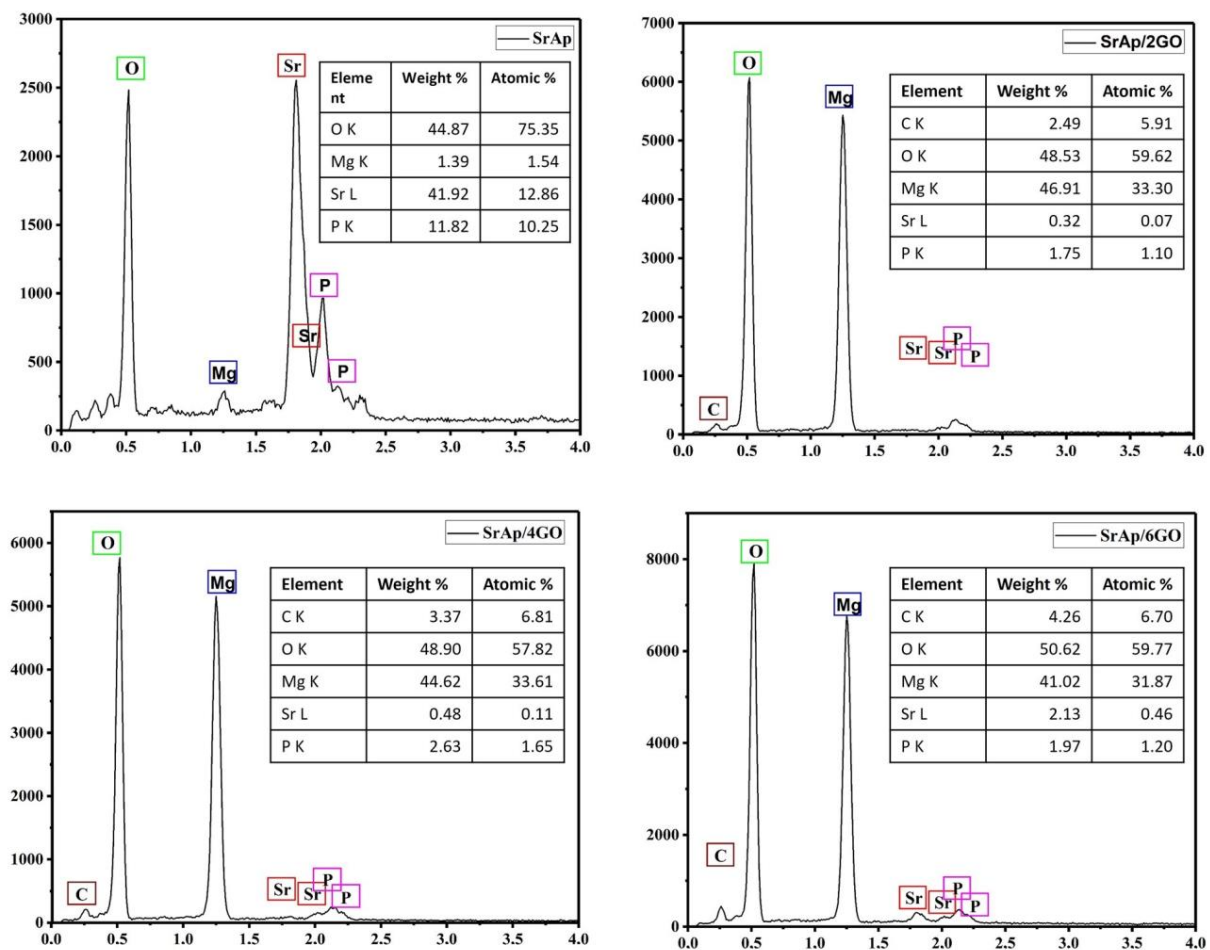


Figure 8. The EDS results of the biocomposite coatings.

The coating thickness was measured as 5.6 μm for only SrAp (GO-free), and 4.84, 4.75, and 4.11 μm for 2, 4, and 6 wt.% GO-containing coatings. The results of the optical profilometry measurements showed that the addition of GO to SrAp coatings on pure Mg reduced the coating thickness. As the GO concentration increased from 2 to 6 wt.%, the coating thickness decreased from 4.84 to 4.11 μm . This reduction in coating thickness is likely due to the increased surface roughness associated with the addition of GO. It is known that high surface roughness can improve the mechanical interlocking and adhesion of the coating to the substrate, as well as promote cell adhesion and proliferation. However, further studies are needed to fully understand the relationship between the coating thickness, surface roughness, and biological properties of these coatings. The surface roughness of the coatings was measured by AFM.

The topological characteristics of GO-free and SrAp/GO biocomposite coatings on the pure Mg surface are presented in Figure 9.

Surface roughness and S_a and S_q values were assessed while analyzing the coatings' entire surface area. The arithmetic mean height of a line's extension to a surface, R_a , is known as S_a . When expressed as an absolute value, it shows how different each point's height is from the surface's arithmetic mean. This variable is frequently used to measure surface roughness. S_q is the extension of R_q to the field and represents the mean square root value of the ordinate values in the defined field. The results of the AFM analysis showed that the surface roughness values of the coatings increased with the increasing GO content of the coatings. Specifically, the S_a and S_q values increased as the GO content increased from 0 to 6%. The roughness values for the GO-free, 2, 4, and 6% GO-added coatings were calculated to be 0.176, 0.335, 0.353, and 0.533 μm for S_a , and 0.241, 0.254, 0.278, and 0.443 μm for S_q , respectively. These findings are consistent with previous studies

showing that increased surface roughness can enhance cell attachment and proliferation, as well as improve the mechanical interlocking between the coating and the bone tissue. Therefore, the high surface roughness of the GO-doped SrAp coatings may have potential applications as a biomaterial for orthopedic implants, where improved osseointegration and corrosion resistance are desired.

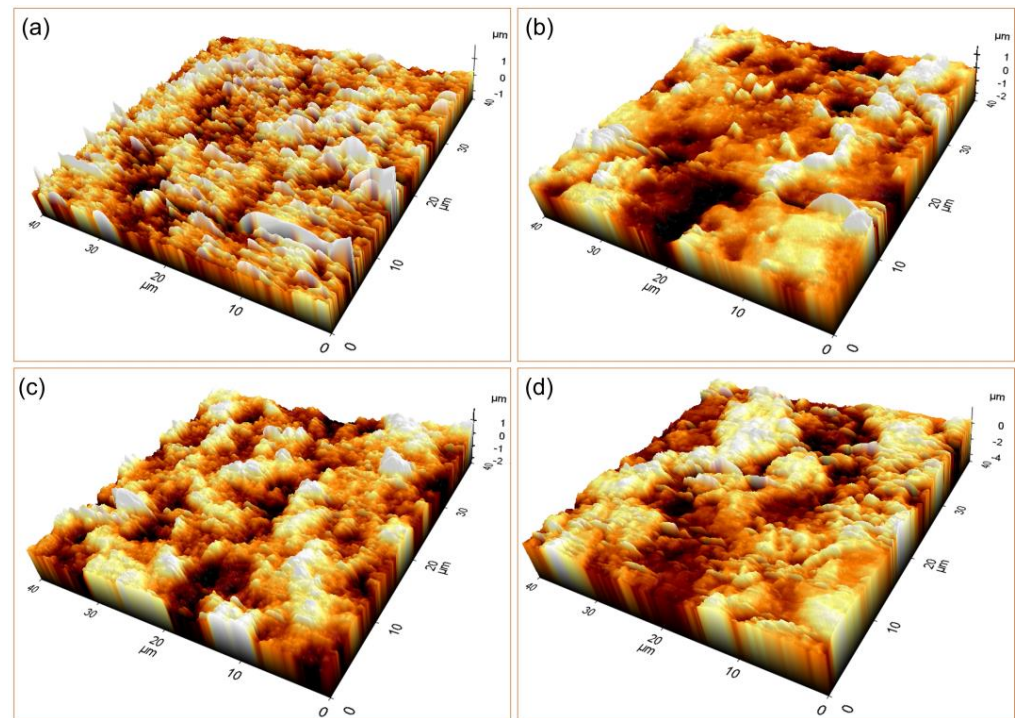


Figure 9. The 3D AFM images of the coated samples with (a) only SrAp (GO-free), and (b) 2, (c) 4, and (d) 6% GO-containing structures.

One of the critical issues in using metallic implants in the human body is ion release, which usually is associated with adverse reactions and can cause significant problems for the patient. The human body consists of a liquid medium containing NaCl, which causes it to act as a corrosive medium for metals. For this reason, it is vital to know the corrosion properties well, especially in metallic implant designs, and to obtain high corrosion resistance in material designs is important trying [37].

Figures 10 and 11 depict the open circuit potential (OCP) and potentiodynamic polarization scanning (PDS) curves, respectively, of the GO-doped SrAp coatings on the pure Mg surfaces. Values for the polarization resistance (R_p), corrosion rates, open current potential value (E_{ocp}), corrosion potential value (E_{corr}), corrosion current densities (I_{corr}), and corrosion rates acquired from PDS curves using the *ElectroChem Analyst* program are compiled in Table 1.

Table 1. Corrosion parameters calculated from PDS curves of the SrAp/GO biocomposite coatings on pure Mg.

| Coating | E_{corr} (mV) | I_{corr} $\mu\text{A}\cdot\text{cm}^{-2}$ | Corr. Rate (mpy) | R_p ($\Omega\cdot\text{cm}^2$) |
|----------|--------------------|---|-----------------------|------------------------------------|
| SrAp | −1632 (± 10) | 43.25 (± 1.95) | 1.040 (± 0.047) | 1306 (± 59) |
| SrAp/2GO | −1515 (± 15) | 5.95 (± 0.75) | 0.143 (± 0.018) | 6402 (± 807) |
| SrAp/4GO | −1448 (± 12) | 5.70 (± 0.50) | 0.137 (± 0.012) | 7123 (± 625) |
| SrAp/6GO | −1239 (± 17) | 4.05 (± 0.45) | 0.097 (± 0.011) | 7286 (± 810) |

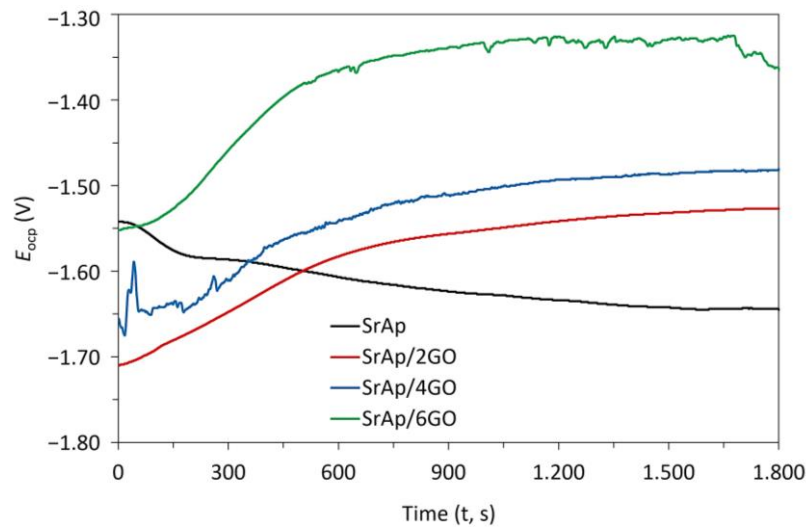


Figure 10. The open circuit potential (OCP) curves of GO-doped SrAp coatings on pure Mg.

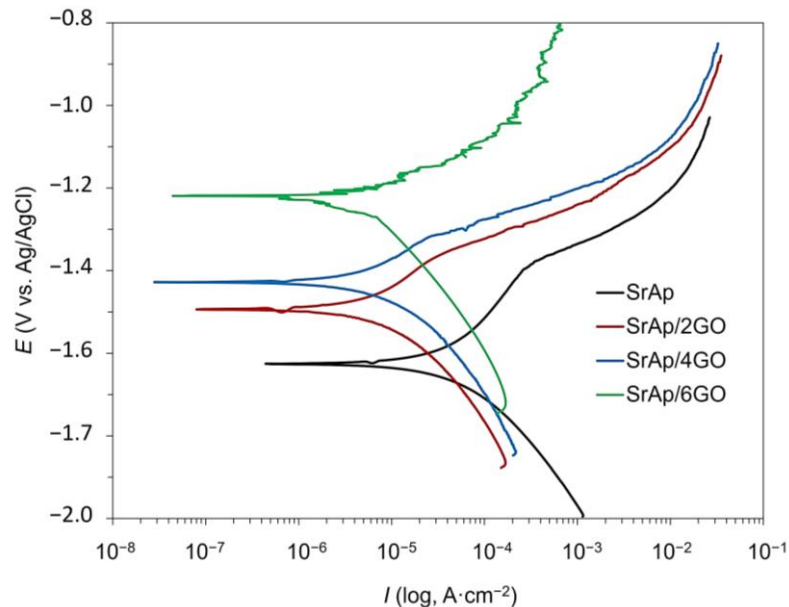


Figure 11. The potentiodynamic polarization scanning (PDS) curves of GO-doped SrAp coatings on pure Mg.

The E_{ocp} of the SrAp, SrAp/2GO, SrAp/4GO, and SrAp/6GO samples were measured to be -1645 , -1537 , -1482 , and -1355 mV, respectively (Figure 10). When the OCP analysis results were evaluated, the OCP curve of the GO-doped SrAp coating decreased with a negative slope and then became stable. In the curves of SrAp/2GO, SrAp/4GO, and SrAp/6GO, fluctuations were observed depending on the GO ratio. The curves became stable with increasing time. The OCP curves of the GO-added samples showed a positive slope. There was no significant change in the E_{corr} values of SrAp and GO-based coatings according to the E_{ocp} values. However, the difference between E_{ocp} and E_{corr} values slightly increased with the increase in GO content in the coating layer. Consistent with the SEM analysis (Figure 4), the fluctuations in the E_{ocp} values that occurred in the SrAp/GO-based coatings were due to the porous structure of the composite coatings and the change in the pore formation and coating characteristics with the GO additive.

The results showed that the addition of GO to the SrAp improved its corrosion behavior. Specifically, the samples with higher amounts of GO exhibited lower corrosion rates and higher polarization resistance compared to the samples without GO. The main

reason for this low corrosion resistance and high corrosion rate in the GO-free SrAp coating may be the porous structure of the coating and the absence of a structure to prevent the corrosion liquid on the Mg substrate surface. In other words, GO-doped composite structures have a more compact coating feature. When GO is added to the coatings, discontinuities may occur in the protective oxide layer, which is expected to occur naturally on the Mg surface [8,18]. Although the SrAp structure shows a porous form in the sample coated with the GO additive, the coating layer is tightly packed, the porosity is generally formed on the surface, and the corrosive liquid with the GO layer is prevented from reaching the Mg substrate. This enhancement can be attributed to the excellent barrier properties of GO, which can hinder the penetration of aggressive species such as Cl^- ions into the coating and reduce the occurrence of localized corrosion. Additionally, the incorporation of GO can facilitate the formation of a more homogeneous and compact coating, which can improve its mechanical and corrosion resistance properties.

Comparing the polarization behaviors of the GO-doped composite coatings revealed a significant decrease in I_{corr} values as the GO content increased, especially at higher rates of GO addition to the composite coating. It is well known that a decrease in I_{corr} in coatings is important because this indicates a reduction in the corrosion rate. In other words, when the I_{corr} values decreased, the coatings became more resistant to corrosion. The I_{corr} values showed that the corrosion current densities decreased with increasing GO content, further supporting the positive impact of GO on the corrosion resistance of the coating.

The addition of GO to the composite coatings significantly increased the values of R_p . The increase in the amount of GO in the composite led to an increase in the R_p value, which is indicative of a change in the morphology of the coating. GO, a monolayer graphite structure with numerous functional groups on both sides, can induce the formation of composite structures in layers and create a dense coating. These structural changes alter the morphology of the SrAp structure on the coated Mg surface and facilitate the formation of an intermediate layer by binding the SrAp structures to the functional GO groups. The resulting multilayer structure based on SrAp and GO has been demonstrated to limit electrolyte leakage, which can reduce the corrosion rate and enhance corrosion resistance. The barrier effect of the graphite layers against liquids in composite structures, which are obtained using GO, graphene nanosheets (GNS), and similar structures, has been reported to be responsible for the observed reduction in the corrosion rate and enhancement of corrosion resistance [8,18,38]. These results indicate that the SrAp/6GO sample had the lowest corrosion rate and highest polarization resistance, suggesting that it has the most promising corrosion behavior among the studied materials.

The SrAp structure was the structure that had the dominant effect in obtaining corrosion resistance in the coating when there was no GO additive in the coating layer. However, this effect on in-vitro corrosion resistance, together with the GO additive, turned into a GO-dependent mechanism and significantly changed the corrosion behavior of the GO structure.

The 6 and 4 wt.% GO-added composite coatings resulted in the lowest I_{corr} and the highest R_p values, respectively; see Table 1. Huang et al. [37] defined it as the ability to produce a successful material that can withstand corrosion for a long time with increased corrosion resistance. This shows that composite materials and coatings doped with GO have high corrosion resistance and are more resistant in the corrosive SBF environment than coatings without GO or with low GO (<1 wt.%). High corrosion rates are typically characterized by surface porosity for coating materials. However, in composite coatings doped using GO and various graphene derivatives, layered and compact coatings increase corrosion resistance. SrAp structures are produced in the interlayers of GO layers while nucleating on the surface. Graphene oxide layers provide a compact and stable form of the coating and allow the formation of a porous structure on the surface that will increase the cell adhesion capability. These compact GO layers form a barrier layer to prevent fluid transmission to the interlayers and substrates while keeping surfaces rough and porous.

As a result, the porous structure occurs only on the surfaces of composite coatings. Table 1 shows that all coatings made with the GO additive had higher in-vitro corrosion resistance. With the increase in the GO ratio, corrosion resistance was increased. The corrosion resistance was found to increase in accordance with this expected behavior.

In SBF, corrosion behavior dependence on the surface morphology of the coating was investigated. The post-corrosion FE-SEM images of pure Mg coated with SrAp/GO biocomposite after the corrosion tests performed at 37 °C in SBF are provided in Figure 12.

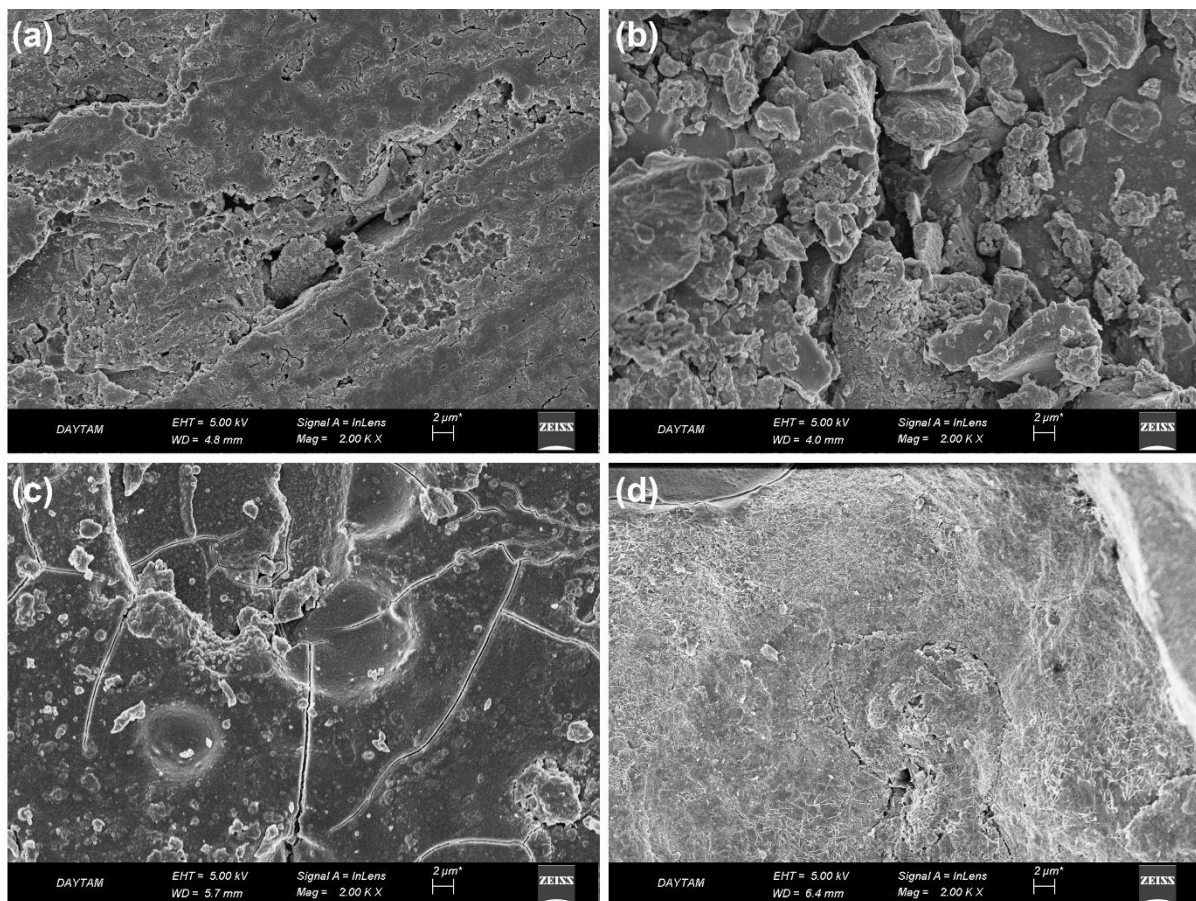


Figure 12. The post-corrosion FE-SEM secondary electron images of biocomposite coatings on pure Mg: (a) SrAp, (b) SrAp/2GO, (c) SrAp/4GO, and (d) SrAp/6GO.

The corrosion damage on the SrAp-based coating was observed in the post-corrosion images. There were locally progressive corrosion traces in the GO. The corrosion liquid caused more corrosion on the composite surfaces containing the GO additive. In the 2 wt.% GO-added coating, although the SrAp and GO-based coatings were still evident on the surface, corrosion damage was high in the coating layer.

The corrosion damage in the 4 wt.% GO coating was spread evenly on the surface as well as in the cracks in the coating. In the SrAp/2GO-based coating, the electrolyte had destroyed the surface locally. This local damage in the coating may be because the layers formed by the GO layer covered the surface and prevented corrosion from occurring on the entire surface. On GO-free surfaces, the propagation of the abrasive liquid into the coating resulted in the formation of these localized corrosions.

The examination of the SrAp/6GO coatings revealed the presence of needle-like and leaf-shaped SrAp grains due to contact with simulated body fluid. Although some areas showed inhibited corrosion, others exhibited corrosion that typically occurs through cracks or tiny spots. The GO layers that inhibited corrosion damage can be seen in Figure 12c,d. In contrast to the SrAp-based coating without GO, the corrosion was inhibited, and leaf-

shaped SrAp seeds remained in the 6 wt.% GO coatings. This unique surface morphology may contribute to enhanced cell adhesion and promote a more advanced surface for biomedical implant applications. These findings highlight the potential of SrAp/6GO coatings for corrosion resistance.

Overall, the results suggest that the addition of GO to Sr-based coatings can be an effective approach to enhance their corrosion resistance, and further studies are warranted to optimize the GO content and investigate the long-term performance of such coatings under more realistic conditions. It is important for researchers to carefully consider the potential consequences and take steps to avoid adverse effects when developing graphene-based biomedical implants. For this, it is essential to consider the potential risks associated with the use of novel materials in biomedical applications and to ensure that the benefits of using such materials outweigh the potential risks. Thus, further research on the investigation of the impact of different graphene oxide concentrations including in-vitro, in vivo, and clinical tests is necessary to fully understand the potential risks of using GO in biodegradable implants and to develop strategies to minimize any adverse effects.

4. Conclusions

In this study, the pure Mg substrate surfaces were coated with strontium apatite (SrAp) and graphene oxide (GO) biocomposite structures using the hydrothermal method. This study aimed to increase the biocompatibility of Mg alloy surfaces and obtain a moderate biodegradation rate. The following conclusions were offered:

- Increasing the GO in SrAp-based coatings significantly enhanced the phase composition and crystallinity, particularly in the coatings with the 6 wt.% GO addition.
- The FT-IR results showed that GO structures had both sp^3 -hybridized and sp^2 -hybridized carbon structures with functional oxygen groups, and the addition of GO led to an increase in C-O functional groups and the formation of more functional groups.
- The SrAp-GO nanocomposite exhibited characteristic absorption bands of phosphate, hydroxyl, and carbonate-based groups, and a strong interaction between SrAp structures and GO formed due to the binding of hydroxyl structures to the functional surface groups of GO during the hydrothermal process.
- The addition of GO layers in SrAp-based coatings led to a composite coating structure with a more compact and coarser SrAp morphology, but with high porosity and rough surfaces, which are preferred for implant applications in biomedical coatings.
- The FE-SEM images showed that with an increasing GO ratio, the size of the SrAp structures decreased significantly and transformed from the microscale to the nanoscale due to the incorporation of GO into the composite, resulting in the formation of surface structures that were coarser and more permeable, while the coating on the surface became denser.
- The EDS analysis indicated that hydrothermal synthesis is a useful method for producing biomedical coatings with controlled chemical ratios, thus supporting the existence of SrAp/GO compounds in coated layers.
- The addition of GO to SrAp coatings improved their corrosion behavior and led to lower corrosion rates and higher polarization resistance compared to the GO-free SrAp coating. The increase in GO content in the composite coatings led to an increase in the polarization resistance (R_p) values, which is indicative of a change in the morphology of the coating.
- The FE-SEM images after the corrosion tests indicated that SrAp/6GO-based coatings have the potential to significantly improve the corrosion resistance and biocompatibility of biomedical implants, due to the presence of needle-like and leaf-shaped SrAp grains and the inhibiting effect of GO layers on corrosion damage.

Author Contributions: O.Y.: Investigation, Formal Analysis, Methodology, Writing—Original Draft; T.G.: Resources, Writing—Original Draft; B.D.: Conceptualization, Supervision, Methodology, Writing—Original Draft, Visualization; M.K.: Validation, Writing—Review and Editing; C.B.: Re-

sources, Writing—Review and Editing; E.A.: Resources, Methodology. All authors have read and agreed to the published version of the manuscript.

Funding: This research received no external funding.

Institutional Review Board Statement: Not applicable.

Informed Consent Statement: Not applicable.

Data Availability Statement: The raw data can be provided if requested.

Conflicts of Interest: The authors have no conflict of interest to declare.

References

1. Hernández-Escobar, D.; Champagne, S.; Yilmazer, H.; Dikici, B.; Boehlert, C.J.; Hermawan, H. Current Status and Perspectives of Zinc-Based Absorbable Alloys for Biomedical Applications. *Acta Biomater.* **2019**, *97*, 1–22. [[CrossRef](#)]
2. Kabir, H.; Munir, K.; Wen, C.; Li, Y. Recent Research and Progress of Biodegradable Zinc Alloys and Composites for Biomedical Applications: Biomechanical and Biocorrosion Perspectives. *Bioact. Mater.* **2021**, *6*, 836–879. [[CrossRef](#)]
3. Hussain, M.; Ullah, S.; Raza, M.R.; Abbas, N.; Ali, A. Recent Developments in Zn-Based Biodegradable Materials for Biomedical Applications. *J. Funct. Biomater.* **2022**, *14*, 1. [[CrossRef](#)]
4. Savaedi, Z.; Motallebi, R.; Mirzadeh, H.; Mehdiavaz Aghdam, R.; Mahmudi, R. Superplasticity of Fine-Grained Magnesium Alloys for Biomedical Applications: A Comprehensive Review. *Curr. Opin. Solid State Mater. Sci.* **2023**, *27*, 101058. [[CrossRef](#)]
5. Zhao, J.; Cui, H.; Gao, Z.; Bi, Y.; Dong, Z.; Li, Y.; Wang, C. Anticorrosive and Antibacterial Smart Integrated Strategy for Biomedical Magnesium. *J. Magnes. Alloy* **2022**. [[CrossRef](#)]
6. Kaseem, M.; Ur Rehman, Z.; Hossain, S.; Singh, A.K.; Dikici, B. A Review on Synthesis, Properties, and Applications of Poly(lactic Acid/Silica Composites). *Polymers* **2021**, *13*, 3036. [[CrossRef](#)]
7. Kaseem, M.; Ramachandriah, K.; Hossain, S.; Dikici, B. A Review on LDH-Smart Functionalization of Anodic Films of Mg Alloys. *Nanomaterials* **2021**, *11*, 536. [[CrossRef](#)] [[PubMed](#)]
8. Yigit, O. Structural, Chemical and Osteogenic Properties of GNS Reinforced Fluorine-Doped Strontiumapatite Coatings on AZ31 Mg Alloys for Potential Biomedical Applications. *Surf. Coat. Technol.* **2022**, *451*, 129031. [[CrossRef](#)]
9. Shapovalova, Y.; Lytkina, D.; Rasskazova, L.; Gudima, A.; Ryabov, V.; Filimoshkin, A.; Kurzina, I.; Kzhyshkowska, J. Bioresorbable Composites Based on Hydroxyapatite Dispersed in Poly-L-Lactide Matrix. *Eur. J. Cancer Suppl.* **2015**, *13*, 49–50. [[CrossRef](#)]
10. Berrio, M.E.; Oñate, A.; Salas, A.; Fernández, K.; Meléndrez, M.F. Synthesis and Applications of Graphene Oxide Aerogels in Bone Tissue Regeneration: A Review. *Mater. Today Chem.* **2021**, *20*, 100422. [[CrossRef](#)]
11. Gurgenc, T. Structural Characterization and Dielectrical Properties of Ag-Doped Nano-Strontium Apatite Particles Produced by Hydrothermal Method. *J. Mol. Struct.* **2021**, *1223*, 128990. [[CrossRef](#)]
12. Khazeni, D.; Saremi, M.; Soltani, R. Development of HA-CNTs Composite Coating on AZ31 Magnesium Alloy by Cathodic Electrodeposition. Part 2: Electrochemical and in-Vitro Behavior. *Ceram. Int.* **2019**, *45*, 11186–11194. [[CrossRef](#)]
13. Sonmez, S.; Aksakal, B.; Dikici, B. Influence of Hydroxyapatite Coating Thickness and Powder Particle Size on Corrosion Performance of MA8M Magnesium Alloy. *J. Alloys Compd.* **2014**, *596*, 125–131. [[CrossRef](#)]
14. Bansal, P.; Singh, G.; Sidhu, H.S. Investigation of Surface Properties and Corrosion Behavior of Plasma Sprayed HA/ZnO Coatings Prepared on AZ31 Mg Alloy. *Surf. Coat. Technol.* **2020**, *401*, 126241. [[CrossRef](#)]
15. Zarka, M.; Dikici, B.; Niinomi, M.; Ezirmik, K.V.; Nakai, M.; Yilmazer, H. A Systematic Study of β -Type Ti-Based PVD Coatings on Magnesium for Biomedical Application. *Vacuum* **2021**, *183*, 109850. [[CrossRef](#)]
16. Wang, T.; Dong, Y.; Xu, Y.; Li, G.; Guo, Y.; Lian, J.; Zhang, Z.; Ren, L. A Calcium Phosphate Coating Improving Corrosion Resistance of the Biodegradable Magnesium Alloy with Graphene Oxide Modifying the Deposition. *Ceram. Int.* **2023**, *49*, 11926–11935. [[CrossRef](#)]
17. Kozelskaya, A.I.; Rutkowski, S.; Frueh, J.; Gogolev, A.S.; Chistyakov, S.G.; Gnedenkov, S.V.; Sinebryukhov, S.L.; Frueh, A.; Egorin, V.S.; Choyzonov, E.L.; et al. Surface Modification of Additively Fabricated Titanium-Based Implants by Means of Bioactive Micro-Arc Oxidation Coatings for Bone Replacement. *J. Funct. Biomater.* **2022**, *13*, 285. [[CrossRef](#)]
18. Yigit, O.; Dikici, B.; Senocak, T.C.; Ozdemir, N. One-Step Synthesis of Nano-Hydroxyapatite/Graphene Nanosheet Hybrid Coatings on Ti6Al4V Alloys by Hydrothermal Method and Their in-Vitro Corrosion Responses. *Surf. Coat. Technol.* **2020**, *394*, 125858. [[CrossRef](#)]
19. Yigit, O.; Dikici, B.; Kaseem, M.; Nakai, M.; Niinomi, M. Facile Formation with HA/Sr-GO-Based Composite Coatings via Green Hydrothermal Treatment on β -Type TiNbTaZr Alloys: Morphological and Electrochemical Insights. *J. Mater. Res.* **2022**, *37*, 2512–2524. [[CrossRef](#)]
20. Ali, A.; Iqbal, F.; Ahmad, A.; Ikram, F.; Nawaz, A.; Chaudhry, A.A.; Siddiqi, S.A.; Rehman, I. Hydrothermal Deposition of High Strength Calcium Phosphate Coatings on Magnesium Alloy for Biomedical Applications. *Surf. Coat. Technol.* **2019**, *357*, 716–727. [[CrossRef](#)]
21. Kavitha, R.J.; Ravichandran, K.; Sankara Narayanan, T.S.N. Deposition of Strontium Phosphate Coatings on Magnesium by Hydrothermal Treatment: Characteristics, Corrosion Resistance and Bioactivity. *J. Alloys Compd.* **2018**, *745*, 725–743. [[CrossRef](#)]

22. Wu, Y.; Wang, Y.; Tian, S.; Jing, Y.; Zhuang, J.; Guo, L.; Jia, D.; Zhou, Y. Hydrothermal Fabrication of RGO/Apatite Layers on AZ31 Magnesium Alloy for Enhanced Bonding Strength and Corrosion Resistance. *Appl. Surf. Sci.* **2019**, *470*, 430–438. [[CrossRef](#)]
23. Yang, C.-W.; Wang, G.-K. Effect of Hydrothermal (Sr)-Hydroxyapatite Coatings on the Corrosion Resistance and Mg²⁺ Ion Release to Enhance Osteoblastic Cell Responses of AZ91D Alloy. *Materials* **2020**, *13*, 591. [[CrossRef](#)] [[PubMed](#)]
24. F2129; Standard Test Method for Conducting Cyclic Potentiodynamic Polarization Measurements to Determine the Corrosion Susceptibility of Small Implant. ASTM International: West Conshohocken, PA, USA, 2017; Volume 86. [[CrossRef](#)]
25. ASTM-G102; Standard Practice for from Electrochemical Measurements. ASTM International: West Conshohocken, PA, USA, 2015; Volume 89, pp. 1–7. [[CrossRef](#)]
26. Gu, X.; Lin, W.; Li, D.; Guo, H.; Li, P.; Fan, Y. Degradation and Biocompatibility of a Series of Strontium Substituted Hydroxyapatite Coatings on Magnesium Alloys. *RSC Adv.* **2019**, *9*, 15013–15021. [[CrossRef](#)]
27. Chen, X.B.; Nisbet, D.R.; Li, R.W.; Smith, P.N.; Abbott, T.B.; Easton, M.A.; Zhang, D.H.; Birbilis, N. Controlling Initial Biodegradation of Magnesium by a Biocompatible Strontium Phosphate Conversion Coating. *Acta Biomater.* **2014**, *10*, 1463–1474. [[CrossRef](#)] [[PubMed](#)]
28. Zhou, S.; Liu, X.; Qian, Z.; Qiao, Y.; Yu, B.; Li, L.; Wang, S.; Qin, Q. Preparation and Characterization of Phosphate Glass–Ceramic Wasteform with Strontium Fluoride. *J. Radioanal. Nucl. Chem.* **2021**, *328*, 217–224. [[CrossRef](#)]
29. Lopes, C.C.; Pinheiro, W.A.; Navarro da Rocha, D.; Neves, J.G.; Correr, A.B.; Ferreira, J.R.M.; Barbosa, R.M.; Soares, J.R.F.; Santos, J.L.; Prado da Silva, M.H. Nanocomposite Powders of Hydroxyapatite-Graphene Oxide for Biological Applications. *Ceram. Int.* **2021**, *47*, 7653–7665. [[CrossRef](#)]
30. Ravi, N.D.; Balu, R.; Sampath Kumar, T.S. Strontium-Substituted Calcium Deficient Hydroxyapatite Nanoparticles: Synthesis, Characterization, and Antibacterial Properties. *J. Am. Ceram. Soc.* **2012**, *95*, 2700–2708. [[CrossRef](#)]
31. Berzina-Cimdina, L.; Borodajenko, N. Research of Calcium Phosphates Using Fourier Transform Infrared Spectroscopy. *Infrared Spectrosc. Mater. Sci. Eng. Technol.* **2012**, *12*, 251–263. [[CrossRef](#)]
32. Dzhurinskiy, D.; Gao, Y.; Yeung, W.-K.; Strumban, E.; Leshchinsky, V.; Chu, P.-J.; Matthews, A.; Yerokhin, A.; Maev, R.G. Characterization and Corrosion Evaluation of TiO₂:N-HA Coatings on Titanium Alloy Formed by Plasma Electrolytic Oxidation. *Surf. Coat. Technol.* **2015**, *269*, 258–265. [[CrossRef](#)]
33. Radha, G.; Venkatesan, B.; Vellaichamy, E.; Balakumar, S. Structural, Mechanical and Biological Insights on Reduced Graphene Nanosheets Reinforced Sonochemically Processed Nano-Hydroxyapatite Ceramics. *Ceram. Int.* **2018**, *44*, 8777–8787. [[CrossRef](#)]
34. Liu, S.; Li, B.; Liang, C.; Wang, H.; Qiao, Z. Formation Mechanism and Adhesive Strength of a Hydroxyapatite/TiO₂ Composite Coating on a Titanium Surface Prepared by Micro-Arc Oxidation. *Appl. Surf. Sci.* **2016**, *362*, 109–114. [[CrossRef](#)]
35. Rajesh, A.; Mangamma, G.; Sairam, T.N.N.; Subramanian, S.; Kalavathi, S.; Kamruddin, M.; Dash, S. Physicochemical Properties of Nanocomposite: Hydroxyapatite in Reduced Graphene Oxide. *Mater. Sci. Eng. C* **2017**, *76*, 203–210. [[CrossRef](#)]
36. Li, M.; Liu, Q.; Jia, Z.; Xu, X.; Shi, Y.; Cheng, Y.; Zheng, Y.; Xi, T.; Wei, S. Electrophoretic Deposition and Electrochemical Behavior of Novel Graphene Oxide-Hyaluronic Acid-Hydroxyapatite Nanocomposite Coatings. *Appl. Surf. Sci.* **2013**, *284*, 804–810. [[CrossRef](#)]
37. Huang, Y.; Zhang, Y.; Li, M.; Yang, H.; Liang, J.; Chen, Y.; Zhang, Y.; Huang, X.; Xie, L.; Lin, H.; et al. Physicochemical, Osteogenic and Antimicrobial Properties of Graphene Oxide Reinforced Silver/Strontium-Doped Hydroxyapatite on Titanium for Potential Orthopedic Applications. *Surf. Coat. Technol.* **2022**, *446*, 128788. [[CrossRef](#)]
38. Asgar, H.; Deen, K.M.; Rahman, Z.U.; Shah, U.H.; Raza, M.A.; Haider, W. Functionalized Graphene Oxide Coating on Ti6Al4V Alloy for Improved Biocompatibility and Corrosion Resistance. *Mater. Sci. Eng. C* **2019**, *94*, 920–928. [[CrossRef](#)]

Disclaimer/Publisher’s Note: The statements, opinions and data contained in all publications are solely those of the individual author(s) and contributor(s) and not of MDPI and/or the editor(s). MDPI and/or the editor(s) disclaim responsibility for any injury to people or property resulting from any ideas, methods, instructions or products referred to in the content.